Dalton Transactions

PAPER

View Article Online
View Journal

Check for updates

Cite this: DOI: 10.1039/d6dt00083e

Janus-faced coordination chemistry of pyridyl-functionalized phosphinines with Cu(I) and Au(I)

Richard O. Kopp, [a] Nathan T. Coles, [a,b] Moritz J. Ernst, [a] Manuela Weber, [a] Benjamin D. Ward [b] and Christian Müller *[a]

The novel 2,6-trimethylsilyl-3,5-(2′-pyridyl)phosphinine has been synthesized and its coordination chemistry with Cu(I) and Au(I) was investigated. Selective binding through either the phosphorus atom or the pendant pyridyl groups was achieved, yielding monomeric, dimeric, and polymeric complexes. The use of copper halides produced rather structurally diverse coordination compounds, with architectures dependent on the type of halide, copper loading, and solvent, whereas Au(I) exclusively formed monomeric species. Quaternization of the ligand with alkylating agents suppressed N-coordination, enabling further study of the resulting cationic derivative with the same metals. These results highlight strongly tuneable coordination behaviour of this new phosphinine scaffold.

Received 12th January 2026,
Accepted 28th February 2026

DOI: 10.1039/d6dt00083e

rsc.li/dalton

Open Access Article. Published on 06 March 2026. Downloaded on 4/1/2026 7:07:11 PM.
This article is licensed under a Creative Commons Attribution 3.0 Unported Licence.

Introduction

2,2′-Bipyridine (**1**, Fig. 1) and its derivatives are ubiquitous ligands in modern chemistry. They play key roles across synthetic organic and inorganic chemistry, supramolecular chemistry, coordination chemistry, and (photo)catalysis.[1,2] Owing to their strong chelating nature, bipyridines readily form stable complexes with a wide range of transition metals, enabling the synthesis of an extensive variety of structurally and functionally diverse metal complexes.

In contrast, phosphorus-containing derivatives of **1** are much less explored, due to their often rather challenging synthesis. In this respect, 2,2′-biphosphinines were first reported by Mathey and Le Floch in 1991, compound **2**, in particular, has been explored with respect to its coordination chemistry.[3,4] Mixed pyridine–phosphinine analogues have also been described since 1982. The access to such compounds, however, required harsh reaction conditions (T > 200 °C) and since then modified synthetic procedures have been developed.[5,6] We could show, for instance, that the classical pyrylium salt route to yield phosphinines can also be applied to the synthesis of **3**, the coordination chemistry of which was subsequently extensively explored.[7–12] Compound **3** resembles a P,N-hybrid ligand, as it contains both a soft (P-atom) and a hard (N-atom) donor atom that can impact the coordination properties and subsequent catalytic applications of the respective coordination compounds.

More recently, we reported the first phosphinine analogues of terpyridine (**4**, **5**, Fig. 2).[13,14] Phosphinine **5** combines the chelating properties of the NPN moiety at the *ortho* position, with the N,N-binding pocket created by the *meta*-pyridyl functionalization within **6**.

The polydentate phosphinines **4** and **5** act as chelating ligands in coordination chemistry. For selective binding of metal fragments to different donor-functionalities, 3,5-bis(2′-pyridyl)phosphinine (**6**), which was reported by Mathey *et al.*,[6] might be a good candidate due to the spatial separation of the phosphorus and nitrogen donors. However, **6** was reported to contain 5% of the 2,5-isomer as a byproduct. Additionally, the phosphorus atom is only weakly sterically shielded, which may allow coordination to larger metal clusters rather than forming well-defined mononuclear coordination compounds.

In this respect, several examples of phosphinine complexes with coinage metals, in particular Au and Cu, have been reported.[9,14–24] For Au(I), most complexes exhibit the typical η^1 binding to the phosphorus atoms, which is to be expected due to the soft nature of Au(I). Our group has reported on the use of phosphinine–Au(I) complexes in a Au(I)-catalyzed reaction.[24] In a report by Siemeling and co-workers intermolecular Au-π interactions between the phosphinine ring of an adjacent monomer were found in the solid state.[16] This is similar to the

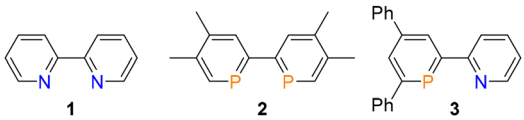

1 2 3

Fig. 1 2,2′-Bipyridine (**1**) and its higher homologues.

[a]Institut für Chemie und Biochemie, Freie Universität Berlin, Fabeckstr. 34/36, 14195 Berlin, Germany. E-mail: c.mueller@fu-berlin.de
[b]School of Chemistry, Cardiff University, Park Place, Cardiff CF10 3AT, UK. E-mail: colesn4@cardiff.ac.uk

Open Access Article. Published on 06 March 2026. Downloaded on 4/1/2026 7:07:11 PM.
This article is licensed under a Creative Commons Attribution 3.0 Unported Licence.

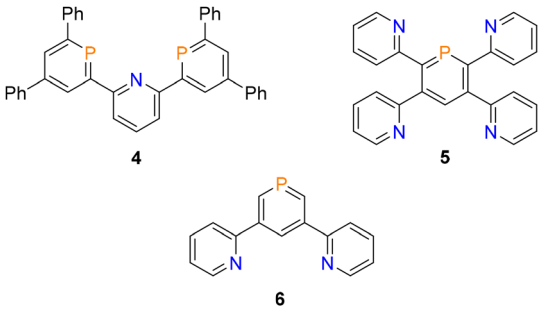

Fig. 2 Hybrid ligands based on phosphinines–pyridines.

type of interaction observed by Mézailles *et al.* for an alkyne functionalized phosphinine, in which an intramolecular interaction was observed.[17] In the case of Cu(I), the coordination behaviour of the aromatic phosphorus heterocycle strongly depends on the substitution pattern of the phosphinine, while the resulting coordination motifs range from coordination polymers to dimeric structures and clusters.[15] Additionally, the phosphinine can also adopt the less common bridging μ_2-P-coordination mode.[9] The only complexes of a mixed phosphinine-pyridine ligand with a coinage metal are reported by our group, where **3**, **4** and **5** bind through both phosphorus and nitrogen atoms.[12–14] Interestingly and despite the presence of multiple donor sites, phosphinine **6** only forms a specific dimeric Cu(I)I complex, regardless of the amount of the Cu(I)X precursor used. An increase in the number of coordination sites does not necessarily lead to a greater diversity of coordination modes.[13]

With a new ligand design, we intended to minimize the multidentate chelation effects at the phosphorus atom while simultaneously integrating an additional coordination site into the molecule to increase the diversity of possible coordination compounds. By exploiting the high regioselectivity observed in the synthesis of phosphinines from diazaphosphinines with $SiMe_3$-functionalised acetylenes, we intended to obtain a multifaceted ligand that can not only coordinate to transition metal salts *via* a single donor site, but also through multiple binding sites in order to access diverse coordination architectures.

Results and discussion

As an initial step, the precursor 1-trimethylsilyl-2-(2′-pyridyl) acetylene (**7**) was synthesized by adapting a microwave-assisted Sonogashira coupling (Scheme 1).[25,26] Notably, earlier literature reports describe compound **7** as a yellow or colourless oil. However, following purification of the crude reaction mixture by trap-to-trap distillation, we obtained acetylene **7** as a crystalline solid.[25–27]

Single crystals suitable for X-ray structural analysis were isolated directly from the condensate. The solid-state molecular structure of **7**, including selected bond lengths and angles, is depicted in Fig. 3. The C(1)–C(2) bond length of 1.2127(10) Å is

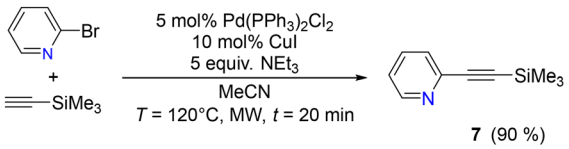

Scheme 1 Synthesis of acetylene **7**.

characteristic of a carbon–carbon triple bond. Furthermore, the Si(1)–C(1)–C(2) and C(1)–C(2)–C(3) bond angles of 176.42(7)° and 177.96(7)°, respectively, are both close to linearity, consistent with the expected geometry of an acetylene moiety.

Subsequently, 2,6-bis(trimethylsilyl)-3,5-bis(2′-pyridyl) phosphinine **8** was synthesized from **7** using an adapted procedure developed by Mathey *et al.* (Scheme 2 and SI).[6,28] The reaction was monitored by means of ^{31}P NMR spectroscopy and, upon completion of the reaction, a single resonance was observed at δ(ppm) = 275.5 (toluene/NEt_3). Crude **8** was purified by several recrystallizations from dry acetonitrile under an argon atmosphere to yield a colorless solid that contained single crystals suitable for X-ray diffraction. The crystallographic characterization of **8** shows that the nitrogen atoms of the pyridyl groups adopt an *anti* conformation (Fig. 4). The phosphinine ring shows bond lengths and angles within error to the closely related 2,6-bis(trimethylsilyl)-3,5-bis(phenyl)phosphinine reported by Le Floch and co-workers.[29] Both compounds show C–P bond lengths of 1.74 Å (**8**: 1.735(2) Å) and bond angles of 106° (**8**: 106.02(10)°) and 126° (**8**: = 125.5(2)°) for C–P–C and C–C(H)–C respectively.

The reactivity of **8** with various copper halides in acetonitrile and under different stoichiometric conditions was examined in more detail. Upon treatment with $CuCl{\cdot}SMe_2$, a dark yellow solution forms immediately. The NMR spectroscopic characterization of the $CuCl{\cdot}SMe_2$ reaction mixture

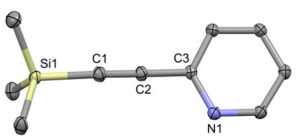

Fig. 3 Molecular structure of **7** in the crystal. Displacement ellipsoids are shown at the 50% probability level; hydrogen atoms are omitted for clarity. Selected bond lengths (Å) and angles (°): C(1)–C(2): 1.2127(10); C(1)–Si(1): 1.8493(7); C(2)–C(3): 1.4417(10); and C(3)–N(1): 1.3502(9). C(1)–C(2)–C(3): 177.96(7); C(2)–C(3)–N(1): 116.76(6); and Si(1)–C(1)–C(2): 176.42(7).

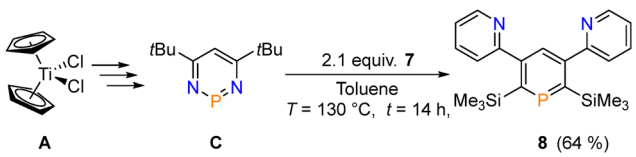

Scheme 2 Synthesis of phosphinine **8** *via* the diazaphosphinine route.

This journal is © The Royal Society of Chemistry 2026

Open Access Article. Published on 06 March 2026. Downloaded on 4/1/2026 7:07:11 PM.
This article is licensed under a Creative Commons Attribution 3.0 Unported Licence.

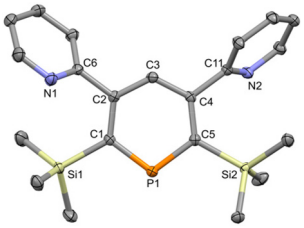

Fig. 4 Molecular structure of **8** in the crystal. Displacement ellipsoids are shown at the 50% probability level; hydrogen atoms are omitted for clarity. Selected bond lengths (Å) and angles (°): C(1)–P(1): 1.735(2); C(1)–C(2): 1.407(3); C(2)–C(3): 1.400(3); C(3)–C(4): 1.396(3); C(4)–C(5): 1.407(3); and C(5)–P(1): 1.7434(19). C(1)–P(1)–C(5): 106.02(10); C(2)–C(3)–C(4): 125.5(2).

showed only minor changes in the chemical shifts relative to the free ligand. Both the ^{1}H and the $^{13}C\{^{1}H\}$ NMR spectra revealed that only one set of pyridyl substituents is present. ESI measurements of this solution in MeCN (see the SI) further revealed fragment ions consistent with a dimeric Cu(I)–Cl–phosphinine species. When 1.1 equivalents of CuBr or CuI are added to a solution of **8** in acetonitrile, no noticeable reaction with the phosphinine occurs at room temperature. However, heating these suspensions to 100 °C results in bright yellow solutions. The ^{31}P NMR spectroscopic analysis of the reaction mixtures in CD_3CN again reveals a slight upfield shift of the phosphinine resonance from δ(ppm) = 272.8 (free **8**) to δ(ppm) = 264.1 (with CuCl) and δ(ppm) = 257.1 (with CuBr). For the CuI reaction, no signal could be detected due to the low solubility of the corresponding complex. The small chemical shift differences between the free phosphinine and its Cu(I) reaction products suggest that phosphorus coordination to Cu(I) does not occur. Instead, binding through the pyridyl nitrogen donors forming the dimeric species **9–11** is the most plausible mode of coordination in this particular case, as depicted in Scheme 3.

Yellow crystals, suitable for single crystal X-ray structure analysis, were obtained for the Cu(I) bromido and Cu(I) iodido complexes **10** and **11**, respectively (Fig. 5 and 6). The crystallographic characterization of **10** and **11** confirms that both coordination compounds adopt dimeric structures. The complexes are isostructural and crystallize in the $P2_1/n$ space group, with the asymmetric unit containing half of a dimer. Each dimer features a planar Cu_2X_2 core, while the remaining coordination sites on copper are occupied by the pyridyl groups of two different phosphinine ligands. Notably, in these structures the ligand bridges both copper centers. This is an uncommon binding mode, as most reported complexes containing bridging pyridyl groups coordinate to only a single copper ion.[30–32] This alternative coordination behavior is attributed to the unusually large N(1)–N(2) separations observed in **10** (5.431(2) Å) and **11** (5.3886(19) Å). Similar binding modes have been reported by Steel and Zhang *et al.* for systems in which the N–N distance exceeds 4 Å.[33,34]

In **10**, the copper ions adopt an almost ideal tetrahedral geometry, with angles of 109.937(13)° for Br(1)–Cu(1)–Br(1′) and 105.24(7)° for N(1)–Cu(1)–N(2′). In contrast, **11** exhibits a more pronounced distortion from tetrahedral geometry due to the larger iodido ligands, reflected in the significantly widened I(1)–Cu(1)–I(1′) angle of 117.071(12)°.

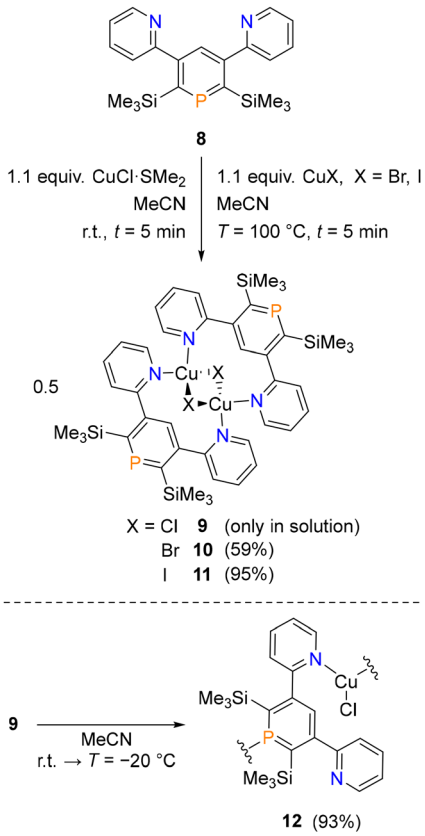

Scheme 3 General reaction scheme for the reaction of **8** with 1.1 equivalents of copper halide (top). Formation of coordination polymer **12** starting from **9** at s–20 °C (bottom).

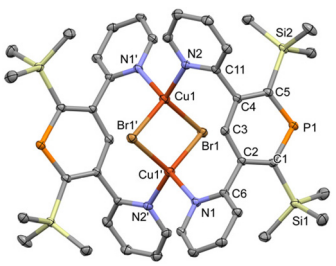

Fig. 5 Molecular structure of **10** in the crystal. Displacement ellipsoids are shown at the 50% probability level; hydrogen atoms are omitted for clarity. Atoms labelled with ′ are generated by the following symmetry operation: 2 − *x*, −*y*, 1 − *z*. Selected bond lengths (Å) and angles (°): Br(1)–Cu(1): 2.4922(3); Br(1)–Cu(1′): 2.5211(4) C(1)–P(1): 1.744(2); C(5)–P(1): 1.742(2); Cu(1)–N(1): 2.0942(17); Cu(1)–N(2′): 2.1124(18); and N(1)–N(2): 5.431(2). Br(1)–Cu(1)–Br(1′): 109.938(11); Cu(1)–Br(1)–Cu(1′): 70.062(11); and N(1)–Cu(1)–N(2′): 105.25(7).

In an attempt to isolate the chloride analogue of **10** and **11** (compound **9**) a concentrated sample of the reaction mixture of phosphinine **8** and $CuCl{\cdot}SMe_2$ was cooled to –20 °C, which

Open Access Article. Published on 06 March 2026. Downloaded on 4/1/2026 7:07:11 PM.
This article is licensed under a Creative Commons Attribution 3.0 Unported Licence.

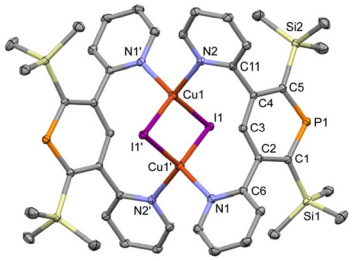

Fig. 6 Molecular structure of **11** in the crystal. Displacement ellipsoids are shown at the 50% probability level; hydrogen atoms are omitted for clarity. Atoms labelled with ′ are generated by the following symmetry operation: 1 − *x*, −*y*, −*z*. Selected bond lengths (Å) and angles (°): C(1)–P(1): 1.7436(16); C(5)–P(1): 1.7445(16); Cu(1)–I(1): 2.6385(2); Cu(1′)–I(1): 2.6699(2); Cu(1)–N(1): 2.1445(14); Cu(1)–N(2′): 2.1190(14); and N(1)–N(2): 5.3886(19). Cu(1)–I(1)–Cu(1′): 62.930(8); I(1)–Cu(1)–I(1′): 117.072(8); and N(1)–Cu(1)–N(2′): 104.22(5).

yielded thin, colorless needles. Single-crystal X-ray diffraction unexpectedly revealed a polymeric structure, markedly different from the proposed dimer **9** observed in solution (Scheme 3). Upon re-dissolution of the crystals in acetonitrile and analysis by ^{31}P NMR spectroscopy, no chemical shift indicative of phosphorus coordination was detected, suggesting that the polymeric species is present only in the solid state.

Compound **12** crystallizes in the space group $P2_1/c$, exhibiting a 1 : 1 stoichiometry between phosphinine **8** and Cu(I)Cl in the asymmetric unit (Fig. 7a and Scheme 3). In contrast to complexes **10** and **11**, no dimerization leading to a four-coordinate Cu(I) center is observed. Instead, in the solid state, complex **12** features a 1D polymeric chain, where each Cu ion adopts a trigonal-planar coordination environment defined by

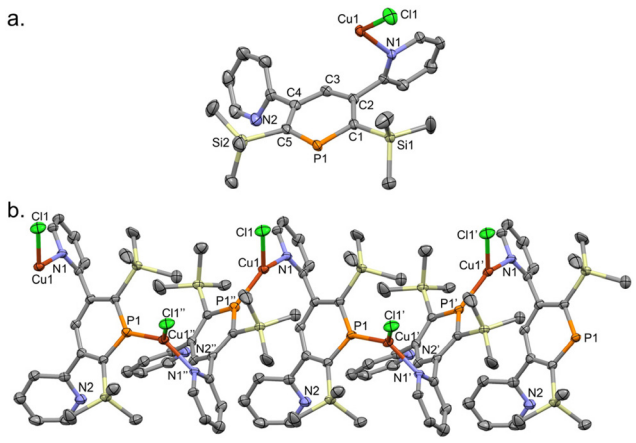

Fig. 7 Asymmetric unit (a) and section of the infinite 1-D chain (b) of coordination polymer **12**. Displacement ellipsoids are shown at the 50% probability level; hydrogen atoms and solvent molecules are omitted for clarity. Atoms labelled with ′ and ″ are generated by the following symmetry operation: ′ (+*X*, 1/2 − *Y*, −1/2 + *Z*); and ″ (+*X*, 1/2 − *Y*, 1/2 + *Z*). Selected bond lengths (Å) and angles (°): Cu(1)–P(1): 2.1685(5); Cu(1)–Cl(1): 2.2266(6); Cu(1)–N(1): 2.0371(16); Cu(1)–Cl(1)–P(1): 125.56(2); Cl(1)–Cu(1)–N(1): 105.85(5); and P(1)–Cu(1)–N(1): 125.97(5).

one phosphorus atom, one nitrogen atom from a single pyridyl substituent, and a terminally bound chlorido ligand (Fig. 7b). The second pyridyl group remains uncoordinated. Terminal binding of Cu(I)–Cl is not unusual. However, CuCl more commonly forms dimeric Cu_2Cl_2 clusters, analogous to its heavier congeners CuBr and CuI. The Cu(1)–Cl(1) bond length of 2.2266(6) Å is slightly shorter than that reported for a comparable trigonal P,N-coordinated Cu(I)Cl complex, which features a Cu–Cl distance of 2.268(2) Å, observed by Jin *et al.*[35] However, to the best of our knowledge, this is the first example of a coordination polymer in which a phosphinine ligand is fully integrated into the polymeric chain rather than merely attached to a polymeric copper halide backbone.[36]

The Cu(1)–N(1) bond length of 2.0371(16) Å is slightly shorter than the corresponding bond in **10**. The copper ion adopts an almost ideal trigonal coordination geometry, with angles of 125.56(2)° for Cu(1)–Cl(1)–P(1) and 125.97(5)° for N(1)–Cu(1)–P(1). For **12**, we propose that the formation of a Cu_2Cl_2 dimer encapsulated by an additional pyridyl group is less favourable than the formation of a polymeric chain. This preference can be partly attributed to the general tendency of halide ligands from Cl^- to I^- to form bridging rather than terminal complexes with metal ions, a behaviour associated with the higher relative polarizability of the heavier halides.[37,38]

Additionally, the absence of a dimeric structure can be attributed to the significantly shorter Cu(I)–Cl bond length, although this contrasts the findings by Li *et al.* who observed a Cu_2Cl_2 containing species. The authors could isolate a Cu_2Cl_2-based phosphine-isoquinolinyl complex with a notably short Cu–Cl bond of 2.3840(7) Å,[39] which are shorter than the Cu–X bonds in the Cu_2Br_2 and Cu_2I_2 analogues **10** and **11**, which measure 2.4921(3) and 2.6386(3) Å, respectively. Such shorter Cu–Cl bonds would produce a more compact Cu_2X_2 core that cannot be accommodated within the N,N-binding pocket of ligand **8** which is dictated by the N–N distance of the pyridine donors. This thereby favors coordination by an additional phosphorus donor, leaving the second pyridyl group uncoordinated and ultimately leading to the formation of the Cu(I)Cl coordination polymer **12**.

To promote coordination at the phosphorus donor, **8** was reacted with 2.7 equivalents of CuBr in MeCN (Scheme 4), which successfully yielded the coordination polymer **13**. The ^{31}P NMR spectrum of the crude reaction mixture displayed a

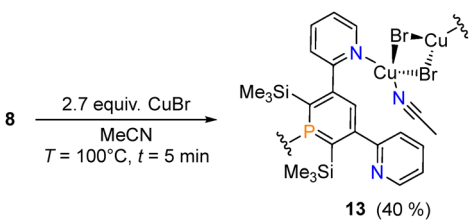

Scheme 4 Reaction of **8** in the presence of MeCN and 2.7 equivalents of CuBr.

This journal is © The Royal Society of Chemistry 2026

Open Access Article. Published on 06 March 2026. Downloaded on 4/1/2026 7:07:11 PM.
This article is licensed under a Creative Commons Attribution 3.0 Unported Licence.

pronounced downfield shift, showing a signal at δ(ppm) = 242.5 (CD_3CN). Slow cooling of the reaction mixture afforded crystalline **13**, and its structure was subsequently confirmed by single crystal X-ray diffraction (Fig. 8).

As in complex **12**, one of the pyridyl groups remains uncoordinated throughout the structure. Instead, an acetonitrile molecule occupies a coordination site, binding to Cu(2) together with the other pyridyl group and two bromido ligands to give a tetrahedral geometry. Cu(1) is coordinated by two Br^- and a phosphorus atom, resulting in a trigonal planar arrangement. The steric constraints imposed by the adjacent trimethylsilyl groups, combined with the significantly greater steric demand of the bromido ligand, favor coordination to smaller copper salt fragments, rather than a pendant coordination to larger copper-halide aggregates and prevent coordination of a second ligand through the phosphorus donor. Phosphinines, in which the phosphorus atom experiences reduced steric shielding, tend to coordinate to larger copper-halide clusters or to polymeric chain motifs.[36,40,41] Compared with the dimer **10**, the Cu_2Br_2 core exhibits a noticeable bend, with a folding angle of 29.418(16)° between the least-squares planes defined by Cu(1)–Br(1)–Cu(2) and Cu(1)–Br(2)–Cu(2). Extension of the asymmetric unit generates a one-dimensional zig-zag chain (Fig. 8).

Because solvent molecules were incorporated into the structure of **13**, attempts were made to react CuBr with **8** in less coordinating solvents, including chloroform, dichloromethane, diglyme, and *o*-difluorobenzene. However, CuBr was insoluble in all of these media, and no reaction was observed. Switching to the more soluble $CuBr{\cdot}SMe_2$ enabled the formation of a new complex. Reactions of **8** with two equivalents of $CuBr{\cdot}SMe_2$ in diglyme or tetrahydrofuran at 120 °C led to the immediate formation of a precipitate, even before complete dissolution of $CuBr{\cdot}SMe_2$ (Scheme 5). Under dilute conditions, this allowed slow crystal growth, resulting in the isolation of single crystals of a new species (**14**) suitable for a single crystal X-ray diffraction analysis (Fig. 9).

As anticipated, no solvent molecules participate in the coordination to the Cu(I) ions. However, in this case the copper halide cluster comprises three crystallographically distinct copper-bromide units. The Cu_3Br_3 core adopts a distorted boat-like geometry, with all three copper centers exhibiting trigonal planar coordination environments. Cu(1) is coordinated by the phosphorus donor and two bromido ligands, while Cu(2) and Cu(3) are each bound to two Br^- and different pyridyl groups. Compared with **13**, complex **14** displays an elongated P–Cu bond, as expected due to the increased size of the Cu–Br core, while no significant lengthening is observed for either the Cu–Br or Cu–N bonds. Notably, although two equivalents of $CuBr{\cdot}SMe_2$ were initially used in the reaction, the NMR spectroscopic analysis of the supernatant revealed the presence of free phosphinine, indicating that all of the copper salt was consumed for the formation of the coordination polymer **14**. Furthermore, the synthesis is not limited to diglyme as the solvent, as the formation of **14** from a THF solution at 120 °C could also be crystallographically confirmed.

Comparing Cu(I)–Cu(I) distances across the obtained complexes **10** (2.8778(5) Å), **11** (2.7710(4) Å) and **13** (2.8255(3) Å), the Cu_3Br_3 cluster displays a separation of Cu(2) and Cu(3) by 2.6893(3) Å, falling significantly below the commonly cited van der Waal radius of 2.80 Å.[42] Comparable complexes with similar Cu–Cu-distances have been interpreted differently in the literature. Chen *et al.* described the situation in a Cu(I)–Cu(I) complex (2.7081(8) Å) as indicative of a 'weak' interaction, whereas other authors find a more definitive terminology for these close contacts.[43–45] More broadly, cuprophilic interactions between Cu(I) centers are generally assumed in the range of 2.4–2.8 Å.[46,47] However, in the case of **14**, photophysical features such as fluorescence, which could indicate a Cu(I)–Cu(I) interaction, were not observed.[40,41,43,45,48] Additional QTAIM analysis (Quantum Theory of Atoms in

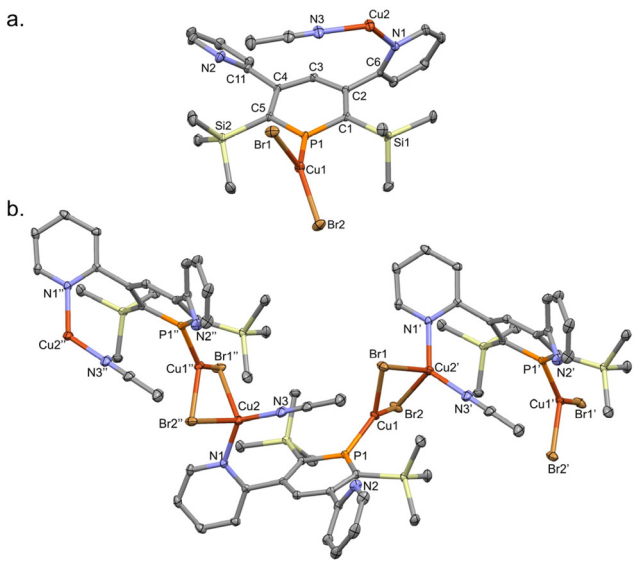

Fig. 8 Asymmetric unit (a) and section of the infinite 1-D chain (b) present in coordination polymer **13**. Displacement ellipsoids are shown at the 50% probability level; hydrogen atoms are omitted for clarity. Atoms labelled with ' and '' are generated by the following symmetry operation: ' (–1/2 + *X*, 1/2 – *Y*, –1/2 + *Z*) and '' (1/2 + *X*, 1/2 – *Y*, 1/2 + *Z*). Selected bond lengths (Å) and angles (°): Br(1)–Cu(1): 2.3902(3); Br(1)–Cu(2): 2.6868(3); Br(2)–Cu(1): 2.3652(3); Br(2)–Cu(2'): 2.4953(3); Cu(1)–P(1): 2.1766(4); Cu(2)–N(1): 2.0113(13); and Cu(2)–N(3): 1.9350(16). Br(1)–Cu(1)–Br(2): 111.993(10); Br(1'')–Cu(2)–Br(2''): 98.992(9); Br(1)–Cu(1)–P(1): 111.608(15); Br(2)–Cu(1)–P(1): 136.092(15); Cu(1)–Br(1)–Cu(2'): 67.338(8); Cu(1)–Br(2)–Cu(2'): 71.030(9); and N(1)–Cu(2)–N(3): 127.14(6).

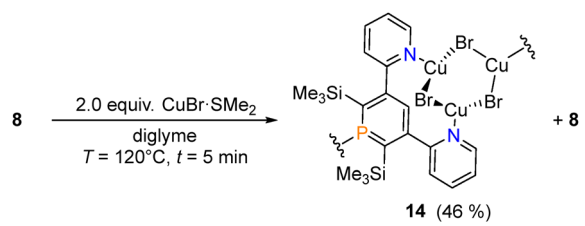

Scheme 5 Reaction of **8** with 2 equivalents of $CuBr{\cdot}SMe_2$ in diglyme.

Open Access Article. Published on 06 March 2026. Downloaded on 4/1/2026 7:07:11 PM.
This article is licensed under a Creative Commons Attribution 3.0 Unported Licence.

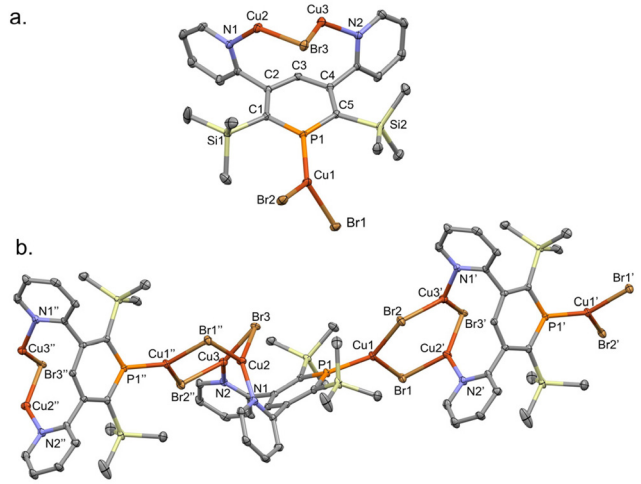

Fig. 9 Asymmetric unit (a) and section of the infinite 1-D chain (b) present in coordination polymer **14**. Displacement ellipsoids are shown at the 50% probability level; hydrogen atoms are omitted for clarity. Atoms labelled with ′ and ″ are generated by the following symmetry operation: ′ (1 + *X*, 3/2 − *Y*, −1/2) and ′ (2 + *X*, 3/2 − *Y*, 1/2 + *Z*). Selected bond lengths (Å) and angles (°): Br(1)–Cu(1): 2.3862(3); Br(1)–Cu(2′): 2.4568(3); Br(2)–Cu(2): 2.3882(3); Br(2)–Cu(3′): 2.4144(3); Br(3)–Cu(1): 2.3778(3); Br(3)–Cu(3): 2.3543(3); Cu(1)–P(1): 2.1843(5); Cu(2)–N(1): 1.9956(14); Cu(3)–N(2): 2.0108(14); and N(1)–N(2): 5.217(6). Cu(1)–Br(1)–Cu(2′): 88.979(9), Cu(1)–Br(2)–Cu(3′): 116.635(10), Cu(3)–Br(3)–Cu(2): 69.262(9), Br(1)–Cu(1)–Br(2): 111.258(10), P(1)–Cu(1)–Br(1): 118.061(15), P(1)–Cu(1)–Br(2): 130.375(15), Br(1″)–Cu(2)–Cu(3): 119.203(10), and Br (3)–Cu(2)–Br(1″):112.416(10).

Molecules) on a model compound, which represents the Cu_3Br_3-containing polymer, does not show any cuprophilic interactions either (Fig. S3 and S4).

Crystals of **14** were dissolved in DMSO-d_6 and, unexpectedly, the ^{31}P NMR spectroscopic analysis indicated the retention of the copper–phosphorus bond in solution. This observation is supported by the pronounced downfield shift of the ^{31}P NMR resonance from δ(ppm) = 272.4 for **8** (in DMSO-d_6) to δ(ppm) = 233.5, accompanied by significant line broadening. Furthermore, the ^{1}H and ^{13}C{^{1}H} NMR spectra display only a single set of pyridyl resonances, consistent with a symmetric binding environment for the two pyridyl substituents in solution. This study shows that variation in the equivalents of copper(I) bromide and the choice of solvent leads to different coordination motifs. Nevertheless, Cu(I) coordination preferentially occurs through the nitrogen atoms, in accordance with Pearson's HSAB concept, while under harsher conditions the less favoured coordination through the phosphorus donor is observed. In the dimeric complexes **10** and **11**, the phosphorus coordination site remains vacant. To gain deeper insight into the coordination propensity at the phosphorus atom, DFT calculations were performed using ORCA 5.0 at the B3LYP/def2-TZVP level of theory, and the frontier molecular orbitals (FMOs) of phosphinine **8** were visualized (Fig. 10). In particular, the presence of an energetically low lying antibonding π* orbital (LUMO) renders phosphinines highly effective ligands for electron-rich transition metals, such as Au(I). In fact, the

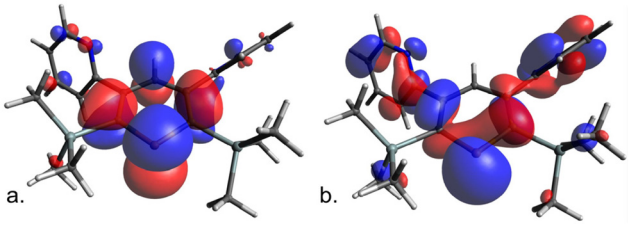

Fig. 10 Visualized frontier molecular orbitals of phosphinine **8**, with the π*-orbital (LUMO) on the left (a) and the lone pair at the phosphorus atom, represented by the HOMO−1, on the right (b). Calculated at the B3LYP def2-TZVP level of theory.

coordination of Au(I) to phosphinines has been explored to quite some extent.[16,17,19,49]

In an attempt to realize bimetallic coordination compounds, a sample of the CuBr complex **10** was first prepared (Scheme 6). The solution was cooled and filtered to remove any excess CuBr that might interfere with the subsequent reaction. The formation of the CuBr complex was verified by NMR spectroscopy prior to the addition of 2.0 equivalents of AuCl·SMe_2. Immediately upon addition of the Au(I) salt, the formation of a colorless, powdery precipitate was observed. Monitoring the supernatant solution by means of ^{31}P NMR spectroscopy revealed no detectable signals, indicating that complex **10** had been completely consumed to form a new compound. All attempts to re-dissolve the resulting solid or to characterize it in solution by dilution were unsuccessful (Scheme 6).

However, upon heating the solid in added tetrahydrofuran, it spontaneously dissolved to afford a yellow solution accompanied by the formation of a fine beige precipitate. Cooling this solution to room temperature yielded a yellow crystalline solid, and single crystals, suitable for crystallographic characterization, were obtained (Fig. 11).

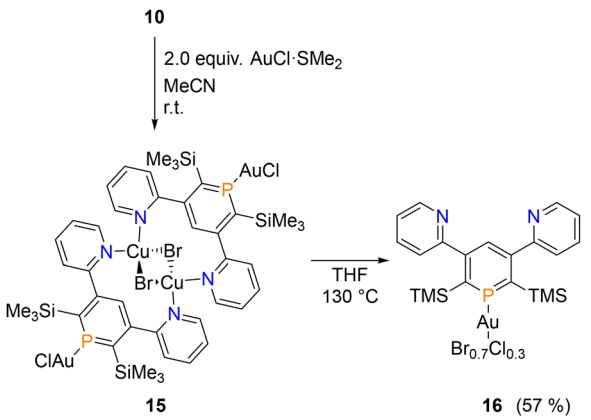

Scheme 6 Reaction of copper bromide complex **10** in the presence of 2.0 equivalents of AuCl·SMe_2 results in the proposed bimetallic complex **15**. Upon heating, **15** decays to complex **16**, which could be characterized by single crystal X-ray diffraction.

This journal is © The Royal Society of Chemistry 2026

Open Access Article. Published on 06 March 2026. Downloaded on 4/1/2026 7:07:11 PM.
This article is licensed under a Creative Commons Attribution 3.0 Unported Licence.

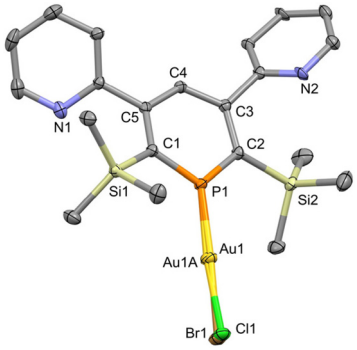

Fig. 11 Molecular structure of **16** in the crystal. Only one part of molecular disorder in the solid state is shown. Displacement ellipsoids are shown at the 50% probability level; hydrogen atoms are omitted for clarity. Selected bond lengths (Å) and angles (°): Au(1)–P(1): 2.2270(15); Au(1)–Br(1); 2.43741(19); P(1)–Au(1A): 2.200(4) Au(1A)–Cl(1): 2.355(9); P(1)–C(1): 1.7199(19), P(1)–C(5): 1.7213(19), P(1)–Au(1)–Br(1): 176.69(7); P(1)–Au(1A)–Cl(1): 171.2(2); C(5)–P(1)–C(1): 111.51(9).

The molecular structure of the new compound in the solid-state revealed the presence of a monomeric gold(I) complex of phosphinine **8** containing both chlorido and bromido ligands, with occupancies of 0.3 and 0.7, respectively (Fig. 11). ESI measurements revealed the detection of both complexes **16-Cl** and **16-Br** simultaneously (see the SI). This assumption is supported by the presence of both chlorido and bromido ligands in the gold complex. The bromido ligand likely originates from the preceding bimetallic species through an anion-exchange process. A ^{31}P NMR spectroscopic analysis of the supernatant solution showed only a very weak resonance attributable to free phosphinine **8**, suggesting that **10** remains almost entirely present in **15**, which is consistent with the strong affinity of phosphorus for Au(I). All attempts to dissolve the gold(I) complex **16** in deuterated solvents for NMR characterization were unsuccessful. Efforts to directly form an Au(I) complex of phosphinine **8** likewise failed under all tested conditions. Reactions with AuCl·SMe$_2$ in acetonitrile, tetrahydrofuran, or dichloromethane produced an immediate yellow solution, followed by the formation of a black precipitate, presumed to be elemental gold. The only tentative indication of a Au–phosphinine intermediate arose from a reaction in dichloromethane, where the supernatant displayed a weak ^{31}P NMR signal at δ(ppm) = 212.7, suggesting a transient coordination species that rapidly decomposes. All subsequent crystallization attempts were unsuccessful. The Au(I)–Cl complex reported by our group for a related phenyl-silyl substituted phosphinine exhibited a comparable ^{31}P{^{1}H} chemical shift of δ(ppm) = 210.6, supporting the assignment of the observed intermediate as the Au(I)Cl complex of **8**.[19]

Our previous studies on pyridyl-functionalized, low-coordinate phosphorus compounds demonstrated that post-synthetic quaternization of the nitrogen donor is an effective strategy to enforce selective coordination through the phosphorus atom, even toward harder metals.[50,51] In addition, we showed that the coordination chemistry of cationic triazaphospholenium salts can be strongly influenced by both the nature of the introduced alkyl group and the counterion. To suppress the donor ability of the pyridyl groups in **8** and to examine the impact of the resulting pyridinium salts on the coordination behaviour, a range of alkylating agents were employed. In an initial attempt phosphinine **8** was suspended in acetonitrile, and the addition of methyl iodide led to immediate dissolution accompanied by a colour change of the solution to intense yellow. Monitoring the reaction showed rapid methylation of one pyridyl group, producing predominantly the mono-pyridinium species along with a smaller amount of the bis-pyridinium salt. To drive the reaction toward the bis-pyridinium, the mixture was heated at 70 °C for two hours (Scheme 7). Concentration of the solution followed by cooling to −20 °C finally afforded the bis(methyl)pyridinium iodide salt **17** as a yellow crystalline solid. Single-crystal X-ray diffraction confirmed the molecular structure of **17** in the crystal (Fig. 12).

The NMR spectroscopic analysis of the bis-pyridinium salt **17** revealed two distinct resonances in the ^{31}P NMR spectrum at δ(ppm) = 281.8 and 282.1, respectively. The rotation of the pyridinium moieties is sterically hindered by the neighboring silyl groups, allowing the detection and characterization of both rotational isomers in solution under ambient conditions (see the SI). To support this assignment, NMR spectroscopic measurements of **17** were performed in the range of 20 °C to 90 °C at intervals of ΔT = 10 °C. Temperatures above 80 °C led to coalescence of both resonances, indicating a high rotational energy barrier as well as the thermal stability of **17** (see the SI).

To achieve coordination with Cu(I) exclusively *via* the phosphorus atom, the bis-pyridinium salt **17** was reacted with CuBr

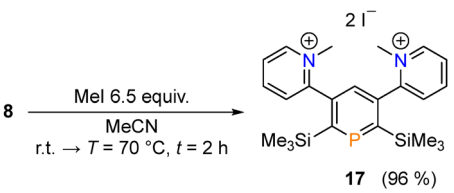

Scheme 7 Reaction of **8** with an excess of MeI results in the bis-methyl pyridinium iodide salt **17**.

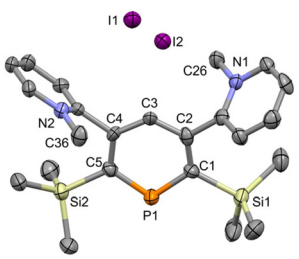

Fig. 12 Molecular structure of **17** in the crystal. Displacement ellipsoids are shown at the 50% probability level; hydrogen atoms and solvent molecules are omitted for clarity. Selected bond lengths (Å) and angles (°): P(1)–C(5): 1.739(6); P(1)–C(1): 1.739(6); N(1)–C(26): 1.461(8); N(2)–C(36): 1.483(8); C(5)–P(1)–C(1): 105.3(2); and C(2)–C(3)–C(4): 123.8(5).

Open Access Article. Published on 06 March 2026. Downloaded on 4/1/2026 7:07:11 PM.
This article is licensed under a Creative Commons Attribution 3.0 Unported Licence.

and CuBr·SMe_2. Surprisingly, the NMR spectroscopic monitoring of the reaction mixtures revealed no new resonances. In addition, an uncharacterized brown precipitate formed after a short time. When coordination was attempted with CuI·SMe_2 (1.5 equivalents) to **17**, a yellow precipitate formed immediately. Analysis of the supernatant solution by ^{31}P NMR spectroscopy revealed no phosphorus resonances, indicating complete consumption of **17**. However, all efforts to dissolve the precipitate were unsuccessful. Next, phosphinine **8** was reacted with varying equivalents of the Meerwein salt $[Et_3O][PF_6]$, which allowed control over the degree of alkylation of **8** (Scheme 8).

For the mono-pyridinium salt **18** a single resonance at δ(ppm) = 278.1 was detected in the ^{31}P NMR spectrum, while the ^{1}H NMR showed two distinct sets of pyridyl moieties. The NMR spectroscopic analysis of the reaction mixture with excess Meerwein salt revealed two resonances in the ^{31}P NMR spectrum at δ(ppm) = 283.1 and δ(ppm) = 284.2, which we attributed to the bis(ethyl)pyridinium salt **19**. After 5 h of reaction time, the two resonances occurred in a final ratio of 1 : 0.6. We found that the solubility of **18** and **19** in acetonitrile was significantly higher than that of the iodide salt **17**. Encouragingly, crystals of both the mono- and bis(ethyl)pyridinium salts suitable for crystallographic analysis were obtained from concentrated acetonitrile/dichloromethane solutions. The molecular structures of **18** and **19** are shown in Fig. 13a and b, together with selected bond lengths and angles.

NMR spectroscopic analysis of a dissolved single crystal of **19** revealed a single ^{31}P resonance at δ(ppm) = 283.1, which is assigned to one rotamer (see the SI). Time-dependent monitoring of this solution by ^{31}P NMR spectroscopy showed the gradual appearance of a second resonance at δ(ppm) = 284.2. After two days, the same 1 : 0.6 ratio was reached (*vide supra*). These findings indicate that interconversion between rotamers occurs more slowly than in the methyl-pyridinium analogue, consistent with increased steric hindrance to C–C bond rotation imposed by the ethyl substituents.

The pyridinium salts **18** and **19** were further reacted with CuBr and CuBr·SMe_2 using various stoichiometries. Despite the presence of one remaining pyridine donor in **18**, no isolable coordination compounds were obtained. Addition of two equivalents of CuBr to a solution of **18** in acetonitrile produced an orange solution, and ^{31}P NMR spectroscopy showed a shift of the resonance from δ(ppm) = 278.1 to δ(ppm) = 266.4, indicating that Cu(I) does not coordinate to the phosphorus atom but rather to the free pyridine substituent (see the SI). However, all attempts to isolate crystals suitable for detailed structural characterization were unsuccessful, and only an amorphous red solid was obtained from saturated solutions at room temperature. In contrast, monitoring reactions of CuBr or CuBr·SMe_2 with **19** by means of ^{31}P NMR spectroscopy revealed no new resonances relative to the free ligand, indicating that no coordination compound forms in solution. This remained the case even in concentrated solutions at low temperature. The only species that could be crystallographically identified was $[Cu(MeCN)_4][PF_6]$.

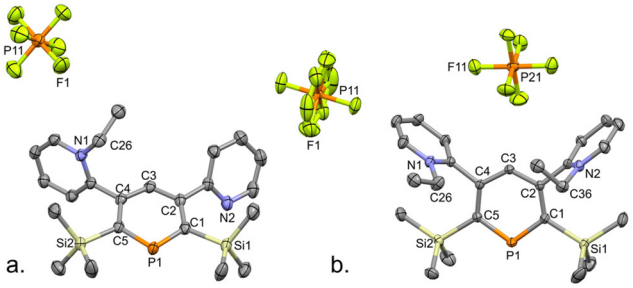

Fig. 13 Molecular structures of the mono- **18** (a) and bis(ethyl)pyridinium salt **19** (b) in the crystal. Displacement ellipsoids are shown at the 50% probability level; hydrogen atoms and solvent molecules are omitted for clarity. Selected bond lengths (Å) and angles (°): for **18**:P(1)–C(1): 1.747(2); P(1)–C(5): 1.741(2); N(1)–C(26): 1.491(3) C(5)–P(1)–C(1): 105.60(11); and C(2)–C(3)–C(4): 124.8(2). For **19**: P(1)–C(1): 1.7423(12); P(1)–C(5): 1.7421(13); N(1)–C(26): 1.5043(19); N(2)–C(36): 1.4920(18), C(5)–P(1)–C(1): 106.26(6); and C(2)–C(3)–C(4): 124.18(11).

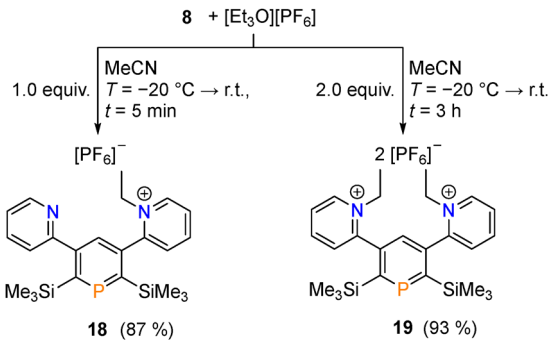

Scheme 8 Reaction of **8** with different equivalents of $[Et_3O][PF_6]$ to the mono- and bis(ethyl)pyridinium salts **18** and **19**, respectively.

To gain deeper insight into the reactivity of the trimethylsilyl–pyridyl-functionalized phosphinine **8** and to evaluate the effect of successive alkylation of its pyridinyl substituents on the frontier molecular orbitals (FMOs), DFT calculations were performed using ORCA 5.0 at the B3LYP/def2-TZVP level of theory (Fig. 14). Calculations were carried out for phosphinine **8**, its corresponding pyridinium salt, and the desilylated compound **5**.

As anticipated, the DFT studies show that phosphinine **8** possesses an enhanced ability to coordinate electron-rich transition-metal cations, which can be attributed to its low-lying LUMO with π symmetry localized at the phosphorus atom. This π* orbital enables effective π back-donation from a metal center. Compared to the TMS-free phosphinine **5**, the electron-donating trimethylsilyl group at the *ortho* position of the phosphorus heterocycle increases the energy of the HOMOs, thereby increasing the σ-donor strength of the phosphorus lone pair.[18,52,53] In contrast, alkylation of the pyridine moieties increases the electron-withdrawing character of the pyridyl-substituents and reduces the electron density within the phosphinine ring.[54] This trend is also reflected in the ^{31}P NMR

This journal is © The Royal Society of Chemistry 2026

Open Access Article. Published on 06 March 2026. Downloaded on 4/1/2026 7:07:11 PM.
This article is licensed under a Creative Commons Attribution 3.0 Unported Licence.

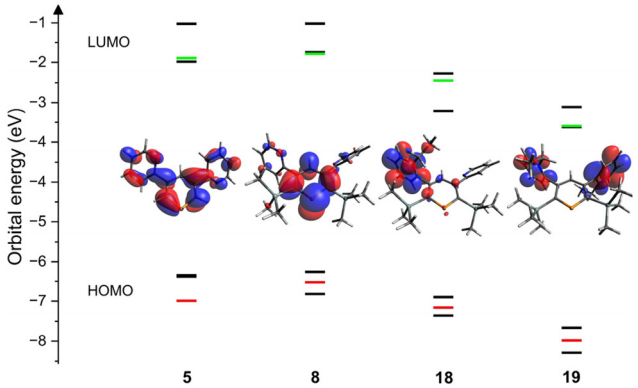

Fig. 14 Frontier Kohn–Sham orbitals and energetic levels (eV) of the desilylated phosphinine **5**, phosphinine **8**, the mono- (**18**) and the bis-ethyl-pyridinium phosphinine salt **19**. The lowest molecular orbital in energy on the phosphorus suitable for π-back-bonding in green and phosphorus lone pair in red. The LUMO was visually represented for comparison purposes. Calculated at the B3LYP def2-TZVP level of theory.

spectra, where resonances shift progressively downfield from **8** to **18** and finally to **19**. Double alkylation not only lowers the energies of the FMOs but also diminishes the overall donor ability. The DFT results further indicate that the LUMO is no longer an antibonding π* orbital localized on the phosphinine ring but is instead predominantly situated on the pyridyl moieties, a feature that may also account for the reduced coordination ability toward Cu(I) salts. Nevertheless, LUMO+1 also lies lower in energy, and this should provide good π-acceptor abilities, particularly towards electron-rich metal cations such as Au(I). To evaluate this, both pyridinium salts **17** and **18** were separately dissolved in acetonitrile and an equimolar quantity of $AuCl{\cdot}SMe_2$ was added (Scheme 9). Upon addition of $AuCl{\cdot}SMe_2$, the reaction mixtures immediately turned intense yellow. The ^{31}P NMR spectroscopic analysis revealed resonances at δ(ppm) = 219.6 and δ(ppm) = 227.8 for the reaction of pyridinium salts **18** and **19**, respectively (see the SI). Comparable results were observed for the reaction of phosphinine **8** with $AuCl{\cdot}SMe_2$ (*vide infra*). The downfield shift of the signal of approximately δ(ppm) = 56 strongly indicates the coordination of gold(I) through the phosphorus atom. Both Au(I) complexes **20** and **21** were characterized by means of NMR spectroscopy. Decomposition of the dilute complexes **20** and **21** was observed rapidly at room temperature, particularly under exposure to light, as indicated by darkening of the solution and the formation of a black precipitate. However, the colorless single crystals of complex **21** exhibited slower decomposition upon light exposure, gradually developing grey inclusions over time.

Concentrated solutions of **20** and **21** in different mixtures of acetonitrile/dichloromethane were prepared. Attempts to crystallize the mono-pyridinium phosphinine–gold complex **20** at −20 °C remained unsuccessful, yielding only a brown amorphous solid. Much to our delight, however, crystals, suitable for single crystal X-ray diffraction analysis, were obtained from a concentrated solution of complex **21** in acetonitrile/dichloromethane (1 : 2) at −20 °C. The molecular structure of **21**, along with selected bond lengths and angles, is depicted in Fig. 15.

Gold complex **21** crystallizes in the orthorhombic space group *P*nma with the asymmetric unit comprising half of the complex salt and half of both $[PF_6]^-$ counter ions, which are located on special positions. Additionally, two half molecules of dichloromethane are incorporated in every asymmetric unit.

The phosphorus–gold bond in **21** has a length of 2.207(2) Å which is only slightly longer than that observed in **16** (2.200(4) Å), which may result from the reduced σ-donor ability of the phosphorus lone pair toward Au(I). Both calculated bond lengths are in line with reported phosphinine–Au(I) bond distances (for example 2.2083(7) Å (ref. 19)). In contrast, the Au–Cl bond in **21** has a length of 2.279(4) Å which is significantly shorter than that in **16** (2.355(9) Å). This can be attributed to the energetically lower-lying LUMO+1 in **21**, which could lead to stronger π back-bonding from the gold center and a concomitant shortened Au–Cl bond.

Notably, all reported crystallographically characterized phosphinine–gold(I) complexes, including **16**, exhibit signifi-

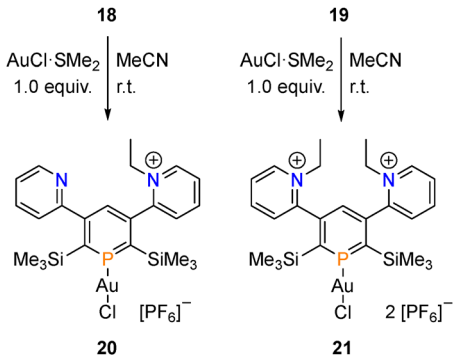

Scheme 9 Reaction of pyridinium salts **18** and **19** with equimolar $AuCl{\cdot}SMe_2$, yielding the corresponding gold chloride complexes **20** and **21**.

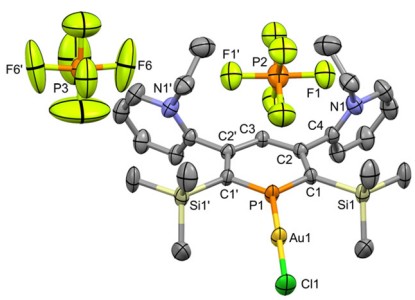

Fig. 15 Molecular structures of pyridinium–phosphinine gold chloride complex **21** in the crystal. Displacement ellipsoids are shown at the 50% probability level; hydrogen atoms and solvent molecules are omitted for clarity. Atoms labelled with (') are generated by the following symmetry operation: 1 + *X*, 1/2 − *Y*, +*Z*; 2 + *X*, 3/2 − Y, +*Z*. Selected bond lengths (Å) and angles (°): Au(1)–P(1): 2.207(2); Au(1)–Cl(1): 2.279(4); P(1)–C(1): 1.718(6), P(1)–Au(1)–Cl(1): 175.5(2); and C(1)–P(1)–C(1'): 112.5(2).

Open Access Article. Published on 06 March 2026. Downloaded on 4/1/2026 7:07:11 PM.
This article is licensed under a Creative Commons Attribution 3.0 Unported Licence.

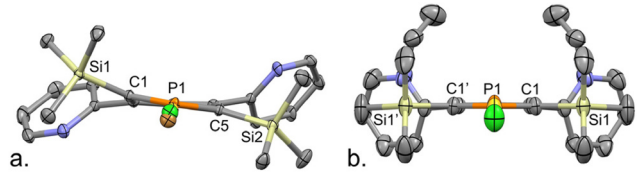

Fig. 16 Molecular structures of phosphinine gold chloride complexes **16** (a) and **21** (b) in the crystal. For **21**, atoms labelled with (′) are generated by the following symmetry operation: 1 + *X*, 1/2 − *Y*, +*Z*; 2 + *X*, 3/2 − *Y*, +*Z*. Displacement ellipsoids are shown at the 50% probability level; hydrogen atoms, counter anions and solvent molecules are omitted for clarity.

cant twisting of the phosphorus heterocycle. We anticipate that donation of the electron density from the Au(I) ion to the π* orbital (LUMO) of the phosphinine destabilizes the π-system of the heterocycle, resulting in the deformation of the P-heterocyclic ring (Fig. 16).

In contrast, complex **21** shows no distortion of the phosphorus heterocycle. DFT calculations indicate that the π* orbital (LUMO+1) involved in Au(I)–P back-bonding exhibits only a p-type coefficient on the phosphorus atom and exhibits no antibonding character within the Si–C–P–C–Si bonding framework. This finding confirms the retained planarity of the phosphinine ring and suggests no major π back-bonding from the metal fragment to any antibonding orbital of the phosphinine ring.

Conclusions

We have designed a pyridyl functionalized phosphinine, taking advantage of the high regioselectivity of the cyclo-addition/cyclo-reversion reaction between diaza-phosphinine and 1-trimethylsilyl-2-(2′-pyridiyl) acetylene (**7**). In this way, we could obtain a ligand featuring spatially separated coordination sites of the pyridine and phosphinine donors. This enabled diverse multi-faceted coordination architecture with Cu(I) and Au(I) halides. The novel 2,6-bis-(trimethylsilyl)-3,5-bis(pyridyl)phosphinine (**8**) exhibits the preference for the formation of dimeric coordination compounds with Cu(I)Br and Cu(I)I, as confirmed crystallographically. Both structures show an encapsulated Cu_2X_2 core within the N,N-binding pocket. An analogous dimeric complex with Cu(I)Cl could not be verified structurally. However, the formation of a coordination polymer, in which the copper center adopts a trigonal coordination environment, could be observed. In the presence of larger quantities of CuBr, coordination polymers with bromido-bridged CuBr clusters were obtained. Our investigations revealed that the amount of CuBr used for the reaction as well as the nature of the solvent dictate the composition of the polymer. Moreover, upon performing the reaction in a phosphinine to CuBr ratio of 1 : 2.7 in acetonitrile, one equivalent of acetonitrile is incorporated into the coordination sphere of Cu(I), resulting in the formation of the phosphinine–Cu-complex **13**. In contrast, the use of solvents with a weaker donor-ability, such as tetrahydrofuran and diglyme, afforded a different coordination polymer (**14**), containing a repeating Cu_3Br_3 unit embedded between the chelating pyridyl groups and the phosphinine donor. Owing to the Janus-faced behavior of ligand **8**, the resulting compounds represent the first coordination polymers in which the phosphinine ligand is fully integrated into the polymer backbone, rather than being merely attached to a Cu(x) framework through pendant coordination. To obtain bimetallic compounds of ligand **8**, the dimeric CuBr complex **10** was reacted with $AuCl{\cdot}SMe_2$ to yield an additional Au(I) coordination *via* the phosphorus atom. The insolubility of the obtained compound prohibited further characterization. Upon heating this solid in THF, the gold complex **16** with a mixed Br/Cl ligand was isolated and structurally characterized by means of single crystal X-ray diffraction. The presence of both anions in the Au(I) complex allowed the proposal of bimetallic complex **15**, which serves as an intermediate *en route* to **16**. To investigate exclusive coordination *via* the phosphorus atom and to tune the electronic properties of the phosphinine, alkylation reactions of the pyridyl substituents with MeI and of $[Et_3O][PF_6]$ with varying stoichiometry were performed. Additionally, DFT calculations on the new phosphinines were carried out in order to reveal the impact of the quaternized pyridyl groups and the TMS-groups on the net-donor and π-acceptance properties of the phosphinines. The alkylation leads to a decrease of the net-donor strength of the phosphorus lone pair, while the π-acceptor capability *via* the LUMO(s) increases. The reaction of the cationic ligands with equimolar amounts of $AuCl{\cdot}SMe_2$ afforded the mono- and bis-ethyl-pyridinium phosphinine gold complexes **20** and **21**, which could be characterized by means of NMR spectroscopy and, in the case of compound **21**, also crystallographically.

Author contributions

R. O. K, N. T. C. and C. M. conceptualized the project and were involved in writing, reviewing and editing of the manuscript. N. T. C. and C. M supervised the project. M. J. E., M. W., and N. T. C. collected crystallographic data and solved and refined the crystal structures. N. T. C. was involved in the validation of the crystallographic data. R. O. K. executed all experimental work, formal analysis and data curation and performed the FMO analysis. N. T. C. and B. D. W. performed the QTAIM analysis.

Conflicts of interest

There are no conflicts to declare.

Data availability

All experimental details and data supporting this article have been included as a part of the supplementary information (SI).

This journal is © The Royal Society of Chemistry 2026

Open Access Article. Published on 06 March 2026. Downloaded on 4/1/2026 7:07:11 PM. This article is licensed under a Creative Commons Attribution 3.0 Unported Licence.

Supplementary information is available. See DOI: https://doi.org/10.1039/d6dt00083e.

CCDC 2502835–2502846 contain the supplementary crystallographic data for this paper.[55a–l]

Acknowledgements

The authors thank Deutsche Forschungsgemeinschaft (DFG) for their generous financial support. The authors would like to thank the HPC Service of FUB-IT, Freie Universität Berlin, for the computing time. Access to the Cardiff University Advanced Research Computing Facility (ARCCA) is gratefully acknowledged.

References

1 C. Kaes, A. Katz and M. W. Hosseini, *Chem. Rev.*, 2000, **100**, 3553–3590.
2 E. C. Constable and C. E. Housecroft, *Coord. Chem. Rev.*, 2017, **350**, 84–104.
3 P. Le Floch, D. Carmichael, L. Ricard and F. Mathey, *J. Am. Chem. Soc.*, 1991, **113**, 667–669.
4 P. Rosa, N. Mézailles, F. Mathey and P. Le Floch, *J. Org. Chem.*, 1998, **63**, 4826–4828.
5 J. Alcaraz, A. Breque and F. Mathey, *Tetrahedron Lett.*, 1982, **23**, 1565–1568.
6 N. Avarvari, P. Le Floch and F. Mathey, *J. Am. Chem. Soc.*, 1996, **118**, 11978–11979.
7 C. Müller, D. Wasserberg, J. J. M. Weemers, E. A. Pidko, S. Hoffmann, M. Lutz, A. L. Spek, S. C. J. Meskers, R. A. J. Janssen, R. A. van Santen and D. Vogt, *Chem. – Eur. J.*, 2007, **13**, 4548–4559.
8 A. Loibl, I. De Krom, E. A. Pidko, M. Weber, J. Wiecko and C. Müller, *Chem. Commun.*, 2014, **50**, 8842–8844.
9 N. T. Coles, A. S. Abels, J. Leitl, R. Wolf, H. Grützmacher and C. Müller, *Coord. Chem. Rev.*, 2021, **433**, 213729.
10 J. Leitl, P. Coburger, D. J. Scott, C. G. P. Ziegler, G. Hierlmeier, R. Wolf, N. P. Van Leest, B. De Bruin, G. Hörner and C. Müller, *Inorg. Chem.*, 2020, **59**, 9951–9961.
11 A. Campos-Carrasco, L. E. E. Broeckx, J. J. M. Weemers, E. A. Pidko, M. Lutz, A. M. Masdeu-Bultó, D. Vogt and C. Müller, *Chem. – Eur. J.*, 2011, **17**, 2510–2517.
12 A. Paderina, R. Ramazanov, R. Valiev, C. Müller and E. Grachova, *Inorg. Chem.*, 2022, **61**, 11629–11638.
13 R. O. Kopp, S. L. Kleynemeyer, L. J. Groth, M. J. Ernst, S. M. Rupf, M. Weber, L. J. Kershaw Cook, N. T. Coles, S. E. Neale and C. Müller, *Chem. Sci.*, 2024, **15**, 5496–5506.
14 C. Müller, E. A. Pidko, M. Lutz, A. L. Spek and D. Vogt, *Chem. – Eur. J.*, 2008, **14**, 8803–8807.
15 M. Shiotsuka, T. Tanamachi, T. Urakawa, M. Munakata and Y. Matsuda, *J. Supramol. Chem.*, 2002, **2**, 211–217.
16 J. Stott, C. Bruhn and U. Siemeling, *Z. Naturforsch., B:J. Chem. Sci.*, 2013, **68**, 853–859.
17 N. Mézailles, L. Ricard, F. Mathey and P. Le Floch, *Eur. J. Inorg. Chem.*, 1999, 2233–2241.
18 M. H. Habicht, F. Wossidlo, T. Bens, E. A. Pidko and C. Müller, *Chem. – Eur. J.*, 2018, **24**, 944–952.
19 M. Rigo, E. R. M. Habraken, K. Bhattacharyya, M. Weber, A. W. Ehlers, N. Mézailles, J. C. Slootweg and C. Müller, *Chem. – Eur. J.*, 2019, **25**, 8769–8779.
20 M. Fraser, D. G. Holah, A. N. Hughes and B. C. Hui, *J. Heterocycl. Chem.*, 1972, **9**, 1457–1459.
21 Y. Mao, K. M. H. Lim, Y. Li, R. Ganguly and F. Mathey, *Organometallics*, 2013, **32**, 3562–3565.
22 Y. Hou, Z. Li, Y. Li, P. Liu, C.-Y. Su, F. Puschmann and H. Grützmacher, *Chem. Sci.*, 2019, **10**, 3168–3180.
23 J. Moussa, L. M. Chamoreau and H. Amouri, *RSC Adv.*, 2014, **4**, 11539.
24 M. Rigo, L. Hettmanczyk, F. J. L. Heutz, S. Hohloch, M. Lutz, B. Sarkar and C. Müller, *Dalton Trans.*, 2017, **46**, 86–95.
25 H. Chiu and I. A. Tonks, *Angew. Chem., Int. Ed.*, 2018, **57**, 6090–6094.
26 Y. Lei, T. Hu, X. Wu, Y. Wu, H. Xiang, H. Sun, Q. You and X. Zhang, *Tetrahedron Lett.*, 2016, **57**, 1100–1103.
27 M. Erdélyi and A. Gogoll, *J. Org. Chem.*, 2001, **66**, 4165–4169.
28 M. Doux, *Nouveaux ligands phosphore soufre: coordination, catalyse et étude théorique*, Chimie de coordination, École Polytechnique X, 2005.
29 A. Moores, T. Cantat, L. Ricard, N. Mézailles and P. Le Floch, *New J. Chem.*, 2007, **31**, 1493–1498.
30 B. W. Skelton, A. F. Waters and A. H. White, *Aust. J. Chem.*, 1991, **44**, 1207–1215.
31 C. O. Kienitz, C. Thöne and P. G. Jones, *Z. Naturforsch.*, 2000, **55b**, 587–596.
32 X. M. Sun, W. H. Ning, J. L. Liu, S. X. Liu, P. C. Guo and X. M. Ren, *Chin. J. Inorg. Chem.*, 2013, **29**, 2176–2182.
33 D. A. McMorran and P. J. Steel, *J. Chem. Soc., Dalton Trans.*, 2002, **17**, 3321–3326.
34 W. Lu, J. Ma, W. Luo, B. Li and T. Zhang, *Inorg. Chim. Acta*, 2016, **442**, 97–104.
35 S. Jin, D. Wang, X. Wang, M. Guo and Q. Zhao, *J. Inorg. Organomet. Polym.*, 2008, **18**, 300–303.
36 S. Giese, K. Klimov, A. Mikeházi, Z. Kelemen, D. S. Frost, S. Steinhauer, P. Müller, L. Nyulászi and C. Müller, *Angew. Chem., Int. Ed.*, 2021, **60**, 3581–3586.
37 K. Fagnou and M. Lautens, *Angew. Chem., Int. Ed.*, 2002, **41**, 26–47.
38 R. A. Widenhoefer and S. L. Buchwald, *Organometallics*, 1996, **15**, 2755–2763.
39 J.-B. Li, Y.-L. Xiao, M.-H. Wu, Y.-H. Jiang, Q.-H. Jin and C.-L. Zhang, *Z. Kristallogr. – New Cryst. Struct.*, 2011, **226**, 97–98.
40 P. Roesch, J. Nitsch, M. Lutz, J. Wiecko, A. Steffen and C. Müller, *Inorg. Chem.*, 2014, **53**, 9855–9859.
41 X. Chen, Z. Li, F. Yanan and H. Grützmacher, *Eur. J. Inorg. Chem.*, 2016, **5**, 633–638.
42 P. P. Power, *Chem. Rev.*, 1999, **99**, 3463–3504.

Open Access Article. Published on 06 March 2026. Downloaded on 4/1/2026 7:07:11 PM.
This article is licensed under a Creative Commons Attribution 3.0 Unported Licence.

43 C.-M. Che, Z. Mao, V. M. Miskowski, M.-C. Tse, C.-K. Chan, K.-K. Cheung, D. L. Phillips and K.-H. Leung, *Angew. Chem., Int. Ed.*, 2000, **39**, 4084–4088.
44 B. Liu, C. Chen, Y. Zhang, X. Liu and W. Chen, *Organometallics*, 2013, **32**, 5451–5460.
45 M. Zafar, V. Subramaniyan, K. U. Ansari, H. Yakir, D. Danovich and Y. Tulchinsky, *Inorg. Chem.*, 2024, **63**, 24466–24481.
46 N. V. S. Harisomayajula, S. Makovetskyi and Y. Tsai, *Chem. – Eur. J.*, 2019, **25**, 8936–8954.
47 D. L. Phillips, C.-M. Che, K. H. Leung, Z. Mao and M.-C. Tse, *Coord. Chem. Rev.*, 2005, **249**, 1476–1490.
48 A. Mensah, J.-J. Shao, J.-L. Ni, G.-J. Li, F.-M. Wang and L.-Z. Chen, *Front. Chem.*, 2022, **9**, 816363.
49 J. Lin, D. S. Frost, N. T. Coles, M. Weber and C. Müller, *Z. Anorg. Allg. Chem.*, 2023, **649**, e202200365.
50 M. Papke, L. Dettling, J. A. W. Sklorz, D. Szieberth, L. Nyulászi and C. Müller, *Angew. Chem., Int. Ed.*, 2017, **56**, 16484–16489.
51 L. Dettling, M. Papke, M. J. Ernst, M. Weber and C. Müller, *Chem. – Eur. J.*, 2024, **30**, e202400592.
52 F. Wossidlo, D. S. Frost, J. Lin, N. T. Coles, K. Klimov, M. Weber, T. Böttcher and C. Müller, *Chem. – Eur. J.*, 2021, **27**, 12788–12795.
53 J. B. Lambert, Y. Zhao, R. W. Emblidge, L. A. Salvador, X. Liu, J.-H. So and E. C. Chelius, *Acc. Chem. Res.*, 1999, **32**, 183–190.
54 P. Wendt, J. Bader, P. L. Waltersmann, J. Schröder, M. Keßler, H. Stammler, B. Neumann, A. Delp, F. Paesler, M. Schulte and B. Hoge, *Chem. – Eur. J.*, 2024, **30**, e202403062.
55 (*a*) CCDC 2502835: Experimental Crystal Structure Determination, 2026, DOI: 10.5517/ccdc.csd.cc2q0dms; (*b*) CCDC 2502836: Experimental Crystal Structure Determination, 2026, DOI: 10.5517/ccdc.csd.cc2q0dnt; (*c*) CCDC 2502837: Experimental Crystal Structure Determination, 2026, DOI: 10.5517/ccdc.csd.cc2q0dpv; (*d*) CCDC 2502838: Experimental Crystal Structure Determination, 2026, DOI: 10.5517/ccdc.csd.cc2q0dqw; (*e*) CCDC 2502839: Experimental Crystal Structure Determination, 2026, DOI: 10.5517/ccdc.csd.cc2q0drx; (*f*) CCDC 2502840: Experimental Crystal Structure Determination, 2026, DOI: 10.5517/ccdc.csd.cc2q0dsy; (*g*) CCDC 2502841: Experimental Crystal Structure Determination, 2026, DOI: 10.5517/ccdc.csd.cc2q0dtz; (*h*) CCDC 2502842: Experimental Crystal Structure Determination, 2026, DOI: 10.5517/ccdc.csd.cc2q0dv0; (*i*) CCDC 2502843: Experimental Crystal Structure Determination, 2026, DOI: 10.5517/ccdc.csd.cc2q0dw1; (*j*) CCDC 2502844: Experimental Crystal Structure Determination, 2026, DOI: 10.5517/ccdc.csd.cc2q0dx2; (*k*) CCDC 2502845: Experimental Crystal Structure Determination, 2026, DOI: 10.5517/ccdc.csd.cc2q0dy3; (*l*) CCDC 2502846: Experimental Crystal Structure Determination, 2026, DOI: 10.5517/ccdc.csd.cc2q0dz4.

This journal is © The Royal Society of Chemistry 2026